Some Characteristics of the End-Extraction PIG Heavy Ion Source with Cold Cathode

By

Michio TOMITA* and Fumio FUKUZAWA*

(Received March 24, 1979)

Abstract

Intensity, emittance, and brightness of the extracted argon beam from the end-extraction PIG ion source were measured as a function of gap-length between the cathode and the extraction electrode. From these data the optimum gap-length was determined. Cathode sputterings of Ta, Al, Cu, and C cathodes were compared. For argon gas the graphite cathode was found to have the longest life-time.

I. Introduction

The end-extraction cold cathode PIG ion source has been favorably used as a heavy ion source of a single stage Van de Graaff accelerator in our laboratory[1]. This type of ion source is a suitable one, because it can be made into a compact size and can be operated at a low power consumption in a low current-high voltage mode. In order to improve the characteristics of the beam extraction and the life-time of the ion source, some measurements were made, looking for a better extraction system and a suitable cathode material.

Firstly, the emittance and the brightness of the extracted beam were investigated for various extraction voltages, discharge voltages and extraction gaps. Secondary, the sputtering yields of four kinds of materials (Cu, Ta, AL, and C) were measured in the PIG discharge with argon gas.

II. Experimental Procedures

Measurements were made on a test-bench. Fig. 1 shows the discharge chamber that was used in the present measurement. The diameter and the thickness of the cathode disc were 18 mm and 1.0 mm, respectively. The exit aperture of the cathode was 1.5 mm in diameter. Fig. 2(a) and 2(b) show schematically the experimental arrangements for the different kinds of measurement which will be mentioned later.

* Department of Nuclear Engineering

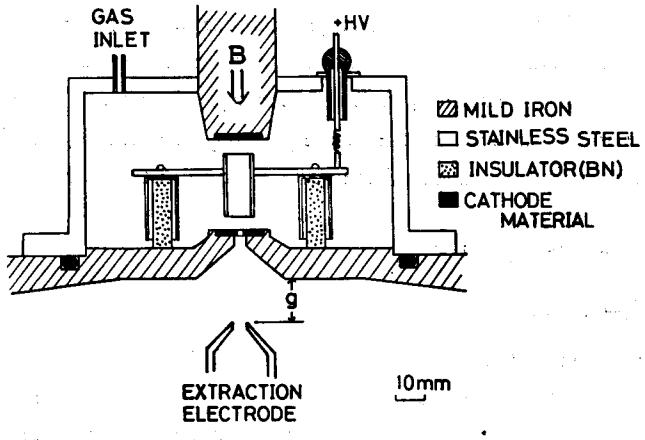

Fig. 1 Cross-sectional view of the discharge chamber.

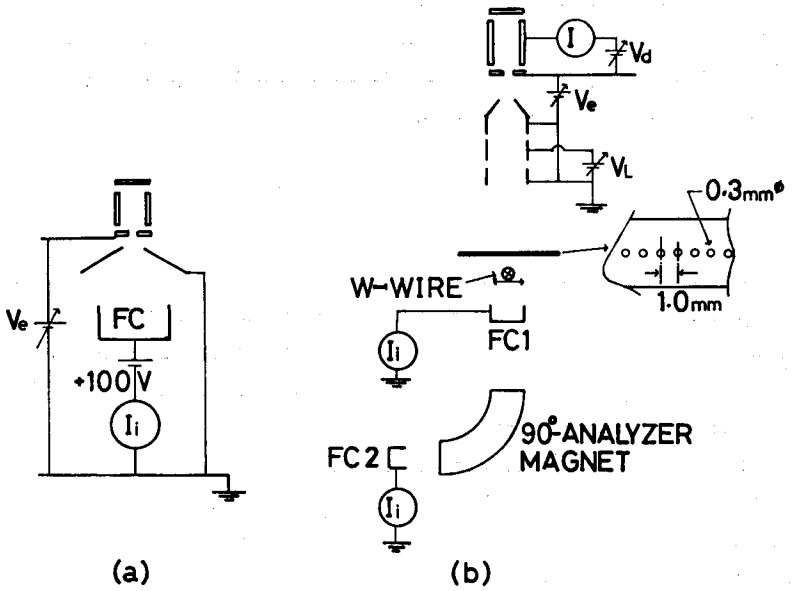

Fig. 2 Schematic showing of the experimental arrangements(a). is for the measurement of the muximum beam current, (b) is used for the measurements of the cathode-sputtering and the characteristics of the extracted beam. For sputtering measurement, the aperture sheet, the tungsten wire, and the Faraday cup (FCl) are removed out.

The beam duct was evacuated by a 6″ oil-diffusion pump at a pressure as low as 3×10^{-6} Torr, while that in the discharge chamber was 6×10^{-4} Torr. When the ion source was operated, gas was fed into the discharge chamber up to the pressure of $(2\text{-}4)\times10^{-3}$ Torr. The pressure P_1 in the discharge chamber in operation was estimated from the measurement of the corresponding pressure P_2 in the beam duct. Because of the small conductance of the exit aperture of the cathode disc, pressure P_2 is negligibly small compared to pressure P_1, and we have the following relation with good accuracy for $P_1 \geqq 1\times10^{-3}$ Torr,

$$P_1/P_2 = 4.4\times10^2 \qquad (1)$$

The value of the constant in the right-hand side of this equation corresponds to the ratio of the pumping speed to the conductance of the exit aperture. This was determined with some values of P_1 and P_2 measured beforehand for the present experimental arrangement.

The magnetic field applied for the PIG discharge was about 0.1 Weber/m^2 on the upper cathode face.

For the sputtering measurement, the composition of the bombarding ions on cath cathode was estimated from the ion spectra of the extracted beam which were measured with a 90°-analyzing magnet. The amount of cathode sputtering was measured with a micro-balance (Saritorius MPR-5).

III. Results and Discussions

(1) Maximum beam current

The maximum beam current available from the ion source was measured with a Faraday-cup placed just behind the extraction electrode. In this case, the extraction electrode was placed closely to the exit aperture of the ion source as shown in Fig. 2 (a). The Faraday-cup was biased to +100 V against the extraction electrode to suppress the secondary electron emission.

The extraction characteristics were measured with Cu, Ta, Al, and C cathodes. Typical results are shown in Fig. 3(a) and 3(b) where the discharge current I_d was used as a parameter. It can be clearly seen in the figures that the total beam current saturates at some extraction voltage, whose value is larger for the larger discharge current. The dashed lines in Fig. 3(b) represent the saturation curves for the discharge voltage, being about two times higher than that giving the solid lines at the same discharge current. Evidently, in this case, saturation occurs faster and the saturated current is larger than in the case of a lower discharge voltage. The saturated beam currents for four cathode materials are plotted as a function of the discharge current in Fig. 4. For each material, the saturated beam current I_i^{max} is proportional

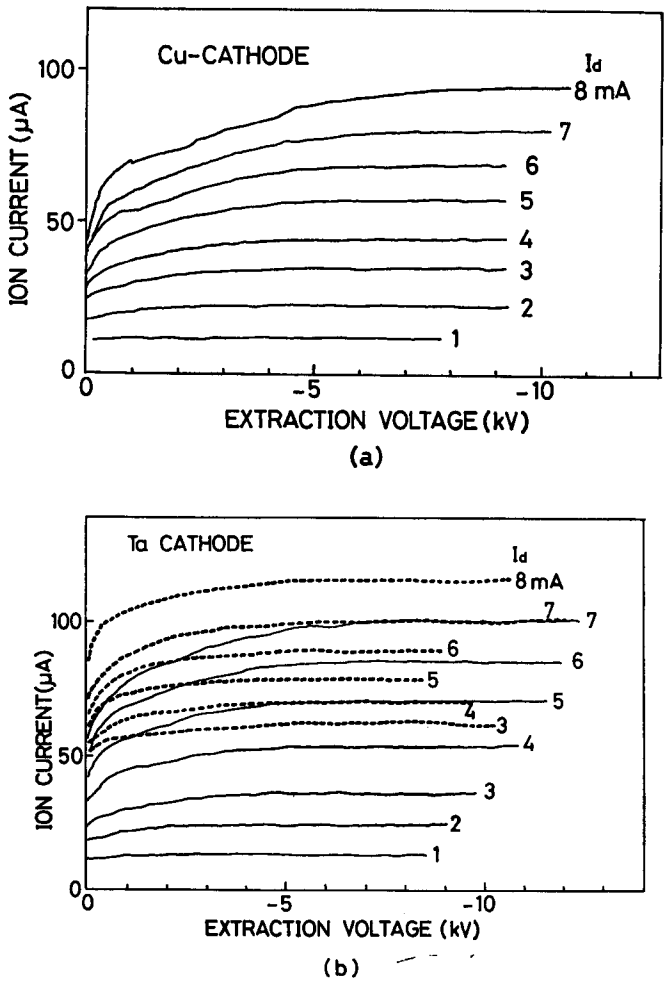

Fig. 3 Saturation properties of the extracted beams which were measured with the arrangement in Fig. 2(a). I_d stands for the discharge current. Dashed lines in (b) represent the saturation curves for higher discharge voltage.

to the discharge current in a range of lower discharge voltage,that is,

$$I_i^{max} = \eta I_d, \tag{2}$$

where η is the proportionality constant. The fact that Eq. (2) holds for four cathode materials with an approximately equal value of η means that the coefficients of the secondary-electron emission are nearly equal for the four materials.

(2) Extraction characteristics

The intensity and the emittance of the extracted beam were investigated in con-

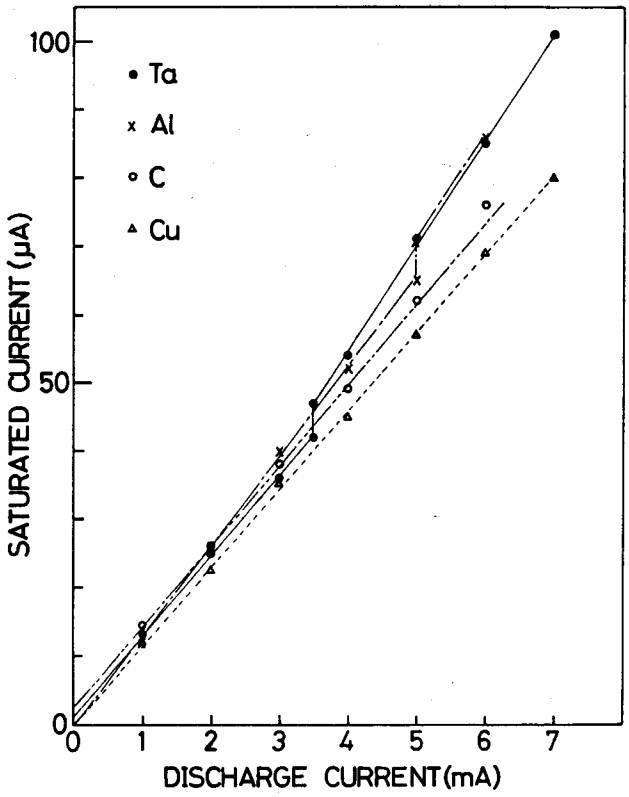

Fig. 4 Variation of the saturation current with the discharge current less than 7 mA. Data are shown for four kinds of the cathode material.

nection with the extraction voltage, the discharge voltage, and the gap-length that was the distance between the extraction electrode and the cathode plate. The experimental arrangement is shown in Fig. 2(b). Measurements on the extracted beam were made after convergence through an einzel lens.

For four gap-lengths, the beam currents are shown in Fig. 5 as a function of the extraction voltage. For the gap-lengths of 16 and 32 mm, the beam current shows saturation properties in the range of extraction voltage of the present experiment, but not for the gap-lengths of 42 and 72 mm. These results come out of the saturation properties mentioned previously. For a small gap, almost all ions which emerged from the exit aperture of the cathode are collected even at a low extraction voltage, while for a larger gap, ion collection becomes insufficient. These features, except for relative intensities, could approximately be reproduced by assuming that the field distribution between the cathode and the extraction electrode is represented by that between the parallel plates. It also assumes that at the exit aperture of the ion source, ions have

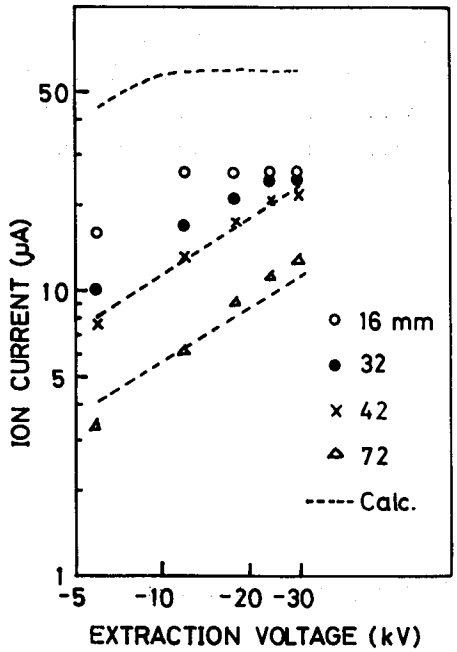

Fig. 5 The ion current for four gap-lengths are shown as a function of the extraction voltage. Ion current was measured with FCl shown in Fig. 2(b), the aperture sheet and W-wire being removed out. The discharge voltage and current were 1.8 kV and 2mA, respectively. The broken lines are calculated ones which are normalized by the 42-mm data.

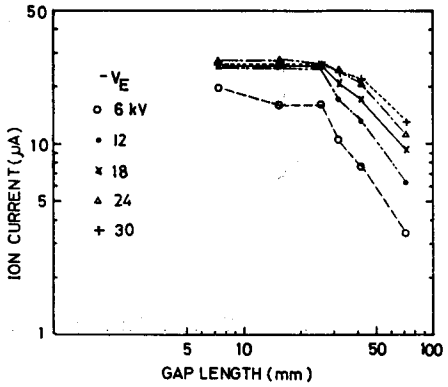

Fig. 6 The ion current for four extraction voltages are shown as a function of the gap-length.

the velocity distribution which was represented as $f(v) = (v/v_0)^{1/4}$, and were emitted isotropically within the diverging angle less than 0.07π radian. Calculated intensities at the gap-lengths of 16, 42, and 72 mm are shown by the broken lines in Fig. 5. Normalization was made for g=42mm data. The calculated value at 16 mm shows an appreciable discrepancy with the experimental one. This discrepancy may be caused by the invalidation of the parallel-plates field distribution at 16 mm. The details of the calculation are described in Appendix A.

Fig. 6 shows the beam current as a function of the gap-length g for various extraction voltages. It is interesting to note that the beam current remains almost constant up to the gap-length of 26 mm. At a larger gap-length, the rate of the decrease of the beam current with a gap-length is larger for a smaller extraction voltage, as is to be expected.

(3) Emittance and brightness

Emittance measurements were made with an aperture-sheet as shown in Fig. 2(b). The current distribution of the beamlet from each aperture was measured by tungsten wire (0.1 mm in diameter) which was driven with a constant speed. The distance between the aperture-sheet and the detection plane on which the tungsten wire

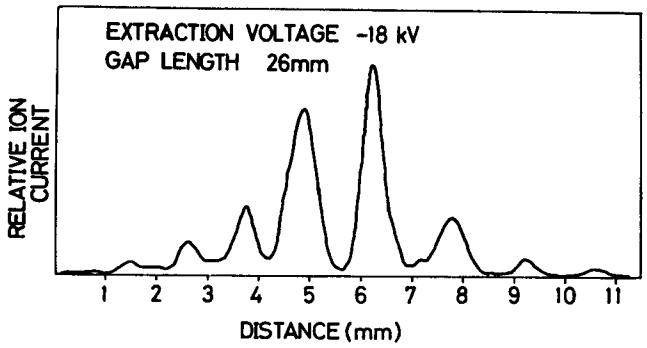

Fig. 7 Current distribution after passing through the aperture sheet.

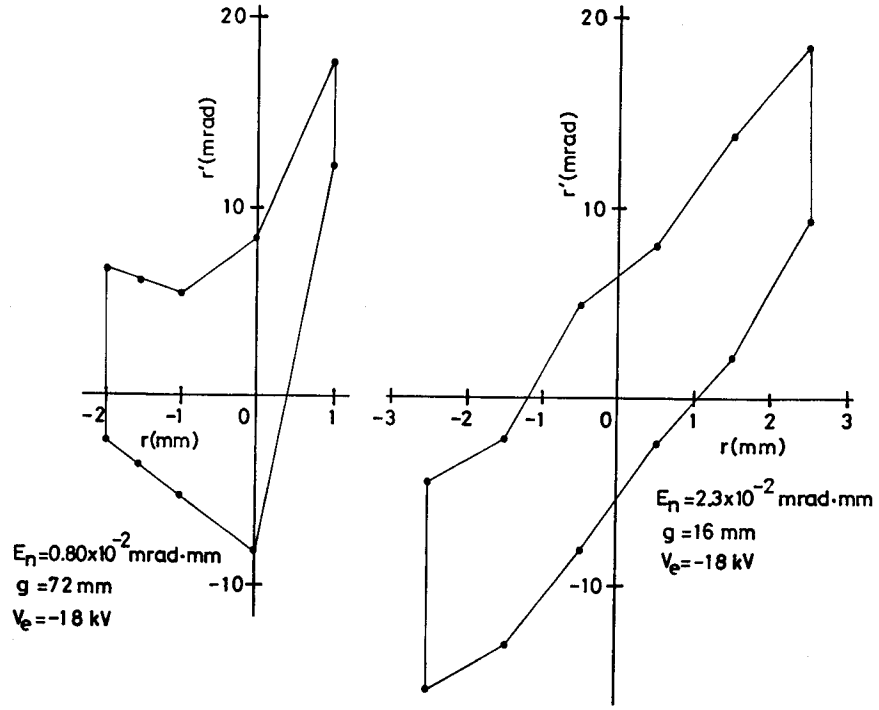

Fig. 8 Typical emittance diagram.

moved was 70 mm. The diameter and the interval of the apertures were 0.3 and 1.0 mm, respectively. A typical current distribution is shown in Fig. 7. From such measurements the emittance diagram can be obtained by the well known procedure[2)3)] which is briefly described in Appendix B. In Fig. 8 are shown two examples for g=16 and 72 mm with the extraction voltage of -18 kV.

The normalized emittance E_n and the normalized brightness B_n, which we briefly call emittance and brightness in the following, were calculated according to the expressions[4)],

$$\begin{aligned} E_n &= \beta\gamma A_e/\pi \\ B_n &= 2I_i/\pi^2 E_n^2 \\ \beta &= v/c \\ \gamma &= (1-\beta^2)^{-1/2}, \end{aligned} \tag{3}$$

where I_i is the beam intensity, A_e the area enclosed by the emittance diagram, v the ion velocity and c the light velocity. Since β is very small compared with unity in the present case (e.g. $\beta \simeq 1\times10^{-3}$ for extraction voltage of -18 kV), γ is taken to be unity with good accuracy.

In Fig. 9, the variation of the emittance with extraction voltage are shown for three gap-lengths. The emittance seems to have no appreciable dependence on the extraction voltage. Thus the variation of brightness with the extraction voltage is almost the same as that of the beam current shown in Fig. 5.

The mean values of the emittance $\bar{E}_n$ over the measured extraction voltages are shown in Fig. 10 as a function of the gap-length. There are two remarkable features. One is that the decrease of $\bar{E}_n$ with a gap-length is much less than the reduction of the solid angle subtended by the extraction electrode opening. Another is that the emittance takes the constant value for g>32 mm. These features were also observed in the case of Ne^+ beams.

The brightness was calculated with the values of $\bar{E}_n$ of Eq. (3) in conjunction with the data shown in Fig. 6, and is shown in Fig. 11 as a function of the gap-length. It is noted in this figure that the maximum takes place at about 32 mm for any extraction voltages. Taking into account the decreasing feature of the beam current mentioned before, the most appropriate gap-length was 30~40 mm for the present arrangement.

Fig. 12 shows the dependences of the emittance and the brightness on the discharge voltages in the case of the gap-length of 32 mm and the extraction voltage of -12 kV. There is no significant variation of the emittance, while the brightness increases linearly with the discharge voltage.

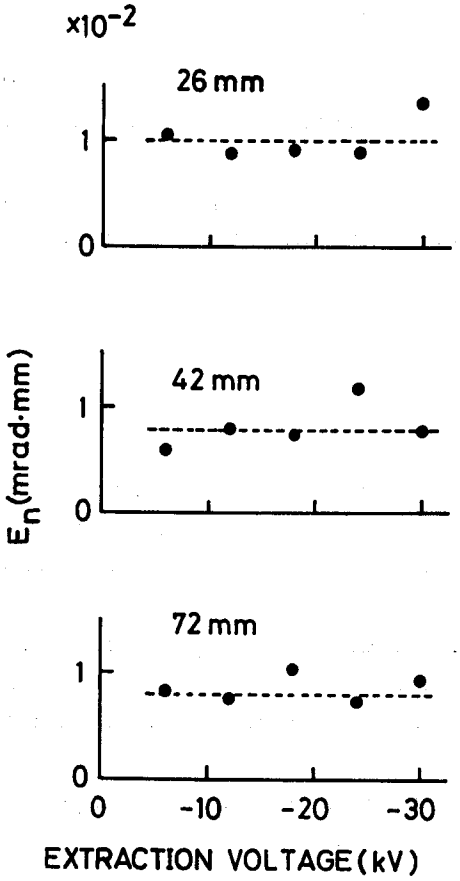

Fig. 9 The normalized emittance are shown for the three gap-lengths as a function of the extraction voltage.

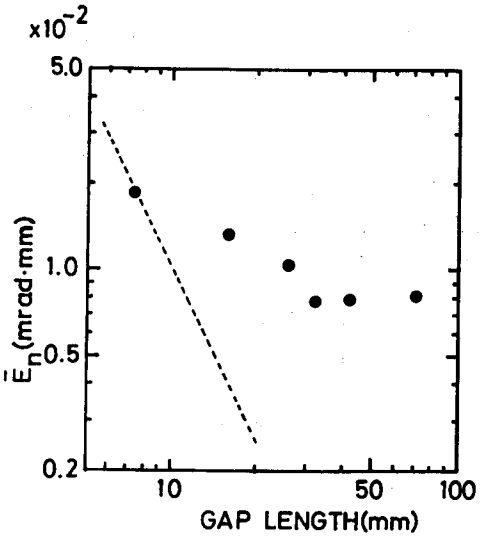

Fig. 10 The dependence of the averaged emittance on the gap-length. The dashed line represents the decrease of the solid angle subtended by the extraction electrode opening.

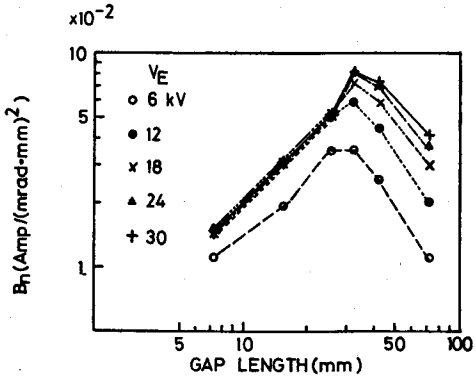

Fig. 11 The normalized brightness as a function of the gap-length.

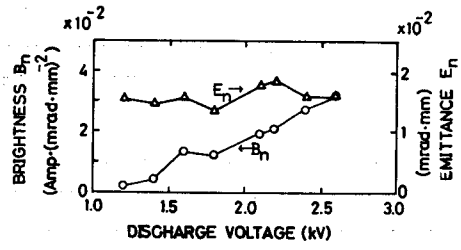

Fig. 12 The dependence of the emittance and the brightness on the discharge voltage.

(4) Cathode sputtering

The life-time of the ion source of this type is determined by the damage of the cathode due to sputtering by the heavy ion bombardment. The sputtering of the cathodes of Cu, Ta, Al, and C were measured in the PIG discharge plasma with argon gas. In the PIG discharge the amount of sputtering of the cathode is expected to be proportional to the number of ions bombarding the cathode as in the case of beam bombarding experiments. Measurements with a different discharge current I_d and time T during which the discharge was held were made for Cu-cathode. The results obtained indicated that the sputtered mass m was proportional to the quantity I_dT as shown in Fig. 13. The discharge current is proportional to the ion current which flows

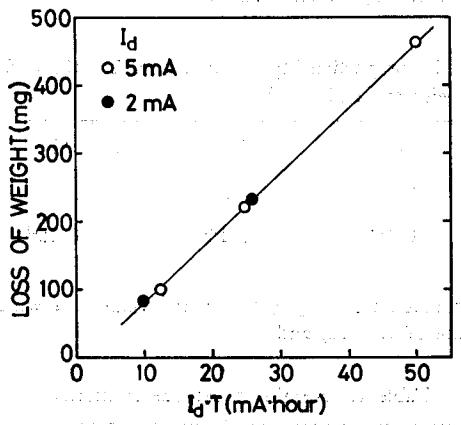

Fig. 13 The weight of the sputtered material is shown as a function of the quantity $I_d \cdot T$.

into the cathode, I_{ion}, and is expressed as

$$I_d = (1+\delta) I_{ion}, \tag{4}$$

where δ is the coefficient of the secondary electron emission for the A-ion bombardment. Thus, the sputtering ratio S(atoms/ion) is written as

$$S = 27\,(m/A)\,(1+\delta)/I_dT \tag{5}$$

where A is the atomic weight of the cathode material, m(mg) the weight of the sputtered material, I_d(mA) the discharge current, and T(hour) the time during which the discharge is held. The values of δ's for Al, Ta, and Cu were reported by Magnuson and Carlson[5] in the case of the 2 keV A^+-ion bombardment. For graphite, the value of the δ's was estimated as follows.

Since the sputtered region on the cathode was almost the same for the four cathodes as regards both the shape and the area, it is reasonable to assume that the

ratio of the extracted beam current I_i^{max} to the ion current flowing into the cathode I_{ion} is independent of the kind of cathode material. That is, if ε is defined as

$$\varepsilon = I_i^{max}/I_{ion}, \tag{6}$$

ε is a constant irrespective of the cathode material. From Eqs. (2), (4), and (6), we obtain the following relation.

$$1+\delta = \varepsilon/\eta. \tag{7}$$

Using the values of η's and δ's for Al, Ta and Cu, one obtains the value of ε as $(1.4\sim1.5)\times10^{-2}$. With this value of ε and the value of η for graphite, the value of δ for graphite was estimated to be 0.08～0.15. These results are listed in Table I.

In the calculation of the sputtering ratios, the value of $(1+\delta)$ was set to be 1.2

Table I Values of the proportionality constant η in Eq. (2) and the coefficient of secondary electron emission δ.

	Cu	Ta	Al	C
η	1.2	1.3	1.3	1.3×10^{-2}
δ	0.15[a)]	0.15[a)]	0.15[a)]	0.08～0.15[b)]

a) ref. 5
b) This was estimated from Eq. (7) with the value of ε which was deduced from the data of Cu, Ta, and Al.

Table II Results of cathode sputtering

MATERIAL	SPUTTERING RATE (mg/mA · hour)	SPUTTERING RATIO (atoms/ion) PRESENT**	OTHERS**	THEORY**	VOLUME CONSUMPTION RATE (cm^3/mA · hour)
Cu	9.5	4.8(2.0)	4.4(2.0)[a)] 3-4(2.0)[b)] 5(2.5)[c)]	4.4(2.0)	1.0×10^{-3}
Ta	7.6	1.3(2.4)	0.9-1.2[b)] (2.4) 1.6 (45)[d)]	3.4(2.4)	0.66
Al	1.8	2.2(2.5)	2-3(2.6)[b)]	2.6(2.5)	0.46
C	0.17	0.41 ～ 0.44 (2.2)	.....	0.22(2.2)	0.09 ～ 0.10

**) Numerical values in the parentheses denote the bombarding energies of A^+ ion in unit of keV.
a) ref. 11
b) Estimated from the data given in ref. 9 by extrapolation.
c) ref. 10
d) ref. 9

for all the cathode materials. This assumtion causes an error, at most 10%. The estimated values of S are listed in Table II together with theoretical values and those obtained by the beam-bombardment experiments. The theoretical values were calculated with the formula derived by Sigmund[6]. A brief account of this calculation is given in Appendix C. Since the discharge is in a high pressure mode[7][8], the potential drop occurs at the plasma sheath formed just adjacent to the cathode surfaces. A large amount of the bombarding ions might be accelerated up to the energy corresponding to this potential drop. Therefore, in this calculation, the energy of the impinging ions was assumed to be eV_d. The sputtering ratios obtained by the PIG discharge are in fairly good agreement with those by the beam-bombardment experiments. The volume-consumption rates are also given in this table.

It is noted that both the sputtering ratio and the volume-consumption rate are minimum for graphite among the four materials. Therefore, graphite is recommended for the cathode material of a PIG ion source.

IV. Summary

(1) The extracted beam current remains almost constant up to the gap-length of 26 mm, after which it decreases with gap-length.

(2) For gap-lengths less than 40 mm, the emittance decreases as the gap-length increases, and for gap-lengths greater than 40 mm the emittance takes the constant value.

(3) From above two results, it becomes clear that the brightness is maximum at the gap-length of 30~40 mm.

(4) At the optimum gap-length, g=32 mm, the emittance does not depend on the discharge voltage nor on the extraction voltage, while the brightness increases as they increase.

(5) The sputtering ratios obtained by the PIG discharge agree well with those by both the beam-bombarding method and the theoretical calculations. With argon gas the graphite cathode has a longer life-time than the Ta-, Al-, and Cu-cathodes.

(6) For graphite, the coefficient of the secondary electron emission due to the A_r^+-ion bombardment was estimated to be 0.08~0.15. This value is nearly equal to those of metals.

Acknowledgment

The authors are grateful to Mr. Akio Itoh for his collaborations.

Appendix A.

We assume that the potential field distribution is represented by that between the

parallel plates.

We now consider the motion of the ions which are ejected at the origin of the coordinate to this electric field with velocity v and the angle θ with respect to the field direction. Under the condition that these particles travel and arrive at the fringe of the aperture (radius b) of the extraction electrode, the initial velocity v_b and the ejection angle θ_b must satisfy the equation

$$(e/m)\,(V/g)\,[b/(v_b \sin\theta)] + v_b \cos\theta = [v_b^2 \cos^2\theta_b + (2e/m)\,V]^{1/2}, \qquad \text{(A-1)}$$

where V, g, e, and m denote the extraction voltage, the gap-length, the charge and the mass of the ions, respectively. As examples, Fig. a-1 shows θ_b as a function of v_b

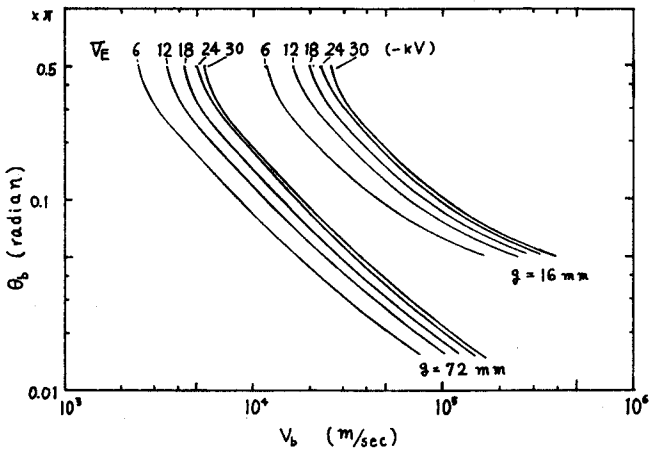

Fig. a-1 relations between the initial velocity and the ejection angle of particles which are to enter the aperture of the extraction electrode. Curves shown are with a radius of the aperture of 2 mm.

for two cases of the gap-lengths with five different extraction voltages. The ions, whose velocity and ejection angle both belong to the lower part of the θ_b-v_b curve, can travel through this aperture.

Let the number of ions dn which arrive at the area of $2\pi x \cdot dx$ on the extraction electrode be

$$dn = 2\pi I(x)\, x \cdot dx, \qquad \text{(A-2)}$$

where I(x) is the number density of the ions at the position x. The integration of Eq. (A-2), from x=0 to x=b, gives the number of ions, n_b, entering the aperture of radius b. Thus we obtain

$$n_b = 2\pi \int_0^b I(x)\, x \cdot dx. \qquad \text{(A-3)}$$

$I(x)x \cdot dx$ can be replaced by $I_0 f(\theta)\sin\theta \cdot d\theta$, where I_0 is the number of ions ejected into the unit solid angle, and $f(\theta)$ is the step function. The function $f(\theta)$ represents the limitation on the divergent angle Θ of the extracted ions, and is defined as follows,

$$\begin{aligned} f(\theta) &= 1 \quad \text{for} \quad \theta < \Theta \\ &= 0 \quad \text{for} \quad \theta > \Theta \end{aligned}$$

Eq. (A-3) is rewritten as

$$\begin{aligned} n_b = 2\pi\int_0^{\theta_b} I_0 f(\theta)\sin\theta \cdot d\theta &= 2\pi I_0(1-\cos\theta_b) \quad \text{for} \quad \Theta > \theta_b \\ &= 2\pi I_0(1-\cos\Theta) \quad \text{for} \quad \Theta < \theta_b \end{aligned}$$

In a practical case, one may take the velocity distribution of the ejected ions as

$$f(\nu) \propto \nu^{\lambda}, \tag{A-5}$$

where $\nu = v/v_0$, and v_0 and λ are the maximum velocity and an adjustable parameter, respectively. Then we can write the expression for the number of ions per unit time, N_b, which enter the aperture of the extraction electrode, as

$$N_b \propto \int_0^{\nu_b} n_b f(\nu)\, d\nu, \quad \nu_b = v_b/v_0 \tag{A-6}$$

Substitution of Eqs. (A-4) and (A-5) into Eq. (A-6) gives the expression

$$\begin{aligned} N_b &= A(1-\cos\theta_b)\nu_b^{\lambda+1} \quad \Theta > \theta_b \\ &= A(1-\cos\Theta)\nu_b^{\lambda+1} \quad \Theta < \theta_b, \end{aligned} \tag{A-7}$$

where A is a constant.

The values of N_b/A at five extraction voltages (-6, -12, -18, -24, and -30 kV) were calculated by use of the $v_b - \theta_b$ curves for the gap-lengths of 16, 42, and 72 mm. If we assume that the values of the parameter λ in Eq. (A-5) and the diverging angle Θ of the ejected beam at the exit aperture were to be 0.25 and 0.157 radian, respectively, the variations of the extracted ion currents which were measured with respect to the extraction voltages were well reproduced. These are shown in Fig. 5 in the text.

Appendix B.

By using the symbols that are shown in Fig. b-1, at each R_j, the mean angle r' subtended between the detector and the aperture relative to the beam axis and its spread $\Delta r'$ are approximately given as

$$r' = (r_j - R_j)/d \tag{B-1}$$

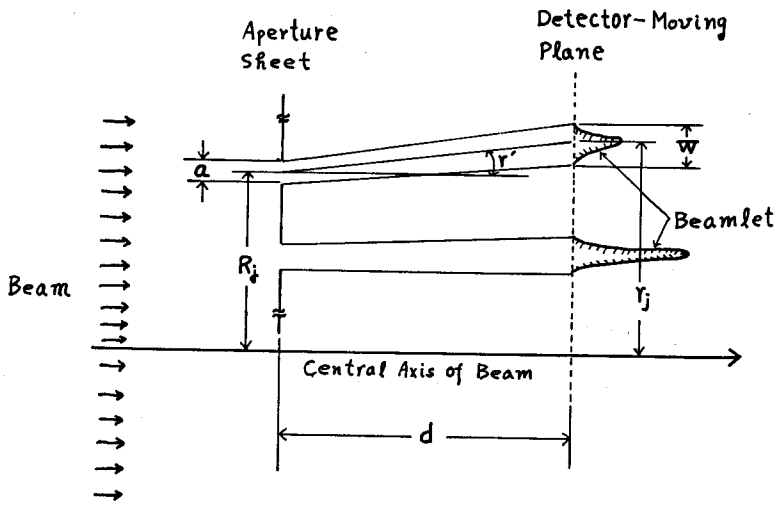

Fig. b-1 Geometry and symbols for emittance measurement.

and

$$\Delta r' = (W-a)/d, \tag{B-2}$$

if $r' \ll 1$. The emittance diagram can be obtained by plotting r' with $\Delta r'$ against R_j. We deal usually with beamlets whose height is greater than one tenth of the maximum height.

Appendix C.

Sigmund[9] has given an expression for the sputtering yield by heavy and medium mass ions with respect to the impinging energy E in the keV region. The sputtering yield S(E) for perpendicular incidence is expressed as (Eq. 96 in ref. 6)

$$S(E) = 0.0420 \cdot \alpha \cdot S_n(E)/U_0 \cdot 10^{-20}, \tag{C-1}$$

where $S_n(E)$ is the nuclear stopping power. α is a factor given as a function of M_2/M_1, where M_1 and M_2 denote the mass number of the incidence and the target atoms, respectively. U_0 is the height of the surface potential of the target material.

The expression by Lindhard et al[13] is adopted for $S_n(E)$, i. e.,

$$S_n(E) = 4Z_1Z_2e^2a[M_1/(M_1+M_2)]s_n(\varepsilon), \tag{C-2}$$

where

$$\varepsilon = aEM_2/[Z_1Z_2e^2(M_1+M_2)],$$

and

$$a = 0.8853a_0(Z_1^{2/3}+Z_2^{2/3})^{-1/2}.$$

Table C-I

	Cu	Ta	Al	C
U_0(eV)	3.51[a)]	8.11[a)]	3.37[a)]	7.43[b)]
α*)	0.33	0.76	0.22	0.18
$a(\times 10^{-11}\text{m})$	1.615	0.949	1.330	1.440

*) Values of α's were read from Fig. 13 in ref. 7
a) ref. 14
b) ref. 15

Table C-II

	Cu	Ta	Al	C
E(keV)	2.0	2.4	2.5	2.2
ε	0.019	0.01	0.040	0.045
$s_n(\varepsilon)$	0.259	0.211	0.311	0.320

Table C-III

	Cu	Ta	Al	C
E(keV)	2.0	2.4	2.5	2.2
S(E) (atoms/ion)	4.4	3.4	2.6	0.22

a_0 is 5.29×10^{-11}m (Bohr radius), and $s_n(\varepsilon)$ is the universal function of ε which is given by Lindhard et al. The values of $s_n(\varepsilon)$ at present were obtained by interpolation from their table. For Cu, Ta, Al, and C, the values of U_0, α, and a were obtained and listed in Table c-I. In Table c-II, the interpolated values of $s_n(\varepsilon)$ are listed together with the impinging energy E and the value of ε.

By substituting the values listed in Table c-I and Table c-II into Eqs. (c-1) and (C-2), the sputtering yield S(E) for each material was obtained and listed in Table c-III with the impinging energies.

References

1) F. Fukuzawa, K. Ogino, M. Tomita, K. Yoshida, K. Norisawa, and M. Sakisaka; Mem. Fac. Engng., Kyoto Univ. **35**, 52 (1973).
2) R. G. Wilson and G. R. Brewer; "Ion Beams", John Willey & Sons Inc. p. 474 (1973).
3) P. H. Rose, R. P. Bastide, N. B. Brooks, J. Airey, and A. B. Wittkower; Rev. Sci. Instr. **35**, 1283 (1964).
4) A. Septier; "Focusing of Charged Particles", Vol. II, Academic Press, p. 150 (1976).
5) G. D. Magnuson and C. E. Carlson; Phys. Rev. **129**, 2403 (1963).

6) P. Sigmund; Phys. Rev. **184**, 383 (1969).
7) W. Schuurman; Physica **36**, 136 (1967).
8) E. B. Hooper, Jr.; Ad. El. and Elect. Phys. **23**, 295 (1969).
9) O. Almen and G. Bruce; Nucl. Instr. Meth. **11**, 257 (1961).
10) N. Laegreid and G. K. Wehner; J. Appl. Phys. **32**, 365 (1961).
11) O. C. Yonts, C. E. Normand, and D. E. Harrison, Jr.; J. Appl. Phys. **31**, 447 (1960).
12) A. L. Southern, W. R. Willis, and M. T. Robinson; J. Appl. Phys. **34**, 153 (1963).
13) J. Lindhard, V. Nielsen, and M. Scharff; Kgl. Danske Videnskab. Selskab., Mat.-Fys. Medd. **36**, No. 10 (1968).
14) Rulf Hultgren, R. L. Orr, D. D. DAndeson, and K. K. Kelley; "Selected Values of Thermodynamic Properties of Metals and Alloys", John Willey & Sons Inc. (1968).
15) D. D. Wagman, W. H. Evans, I Halow, and R. M. Dudley; "American Institute of Physics Handbook", 2nd ed. McGraw-Hill, p. 4-176.